Narrow Stimulated Resonance Raman Scattering and WGM Lasing in Small Conjugated Polymer Particles for Live Cell Tagging and Tracking

Bastian Haehnle, Markus Lamla, Konstantin M. J. Sparrer, Malte C. Gather, and Alexander J. C. Kuehne*

Conjugated polymer particles are brightly fluorescing and stable materials for live cell imaging. Combination of conjugated polymers with a whispering gallery mode (WGM) resonator allows laser emission from microscale particles. Once internalized by cells, the mode pattern of the laser emission can be used for tagging and tracking, as each laser spectrum represents a bar code to identify individual cells. However, currently these particle systems are limited by their large size, which might interfere with cellular functions. Here, stimulated resonance Raman scattering (SRRS) in small conjugated polymer microparticles is presented as a new method for generating narrow emission as an alternative to WGM-based laser emission. This opens up spectral range for multiplexing optical readout and multicolor imaging of live cells. The synthesis of monodisperse micrometer-sized poly(fluorene-*co*-divinylbenzene) particles is discussed and their WGM and SRRS emission are characterized. Finally, how these particles and their emission can be employed in live cell imaging and tagging is showcased.

B. Haehnle, Dr. M. Lamla, Prof. A. J. C. Kuehne
Institute of Organic and Macromolecular Chemistry
Ulm University
Albert-Einstein-Allee 11, 89081 Ulm, Germany
E-mail: alexander.kuehne@uni-ulm.de
Dr. K. M. J. Sparrer
Institute of Molecular Virology
Ulm University Medical Center
89081 Ulm, Germany
Prof. M. C. Gather
SUPA
School of Physics and Astronomy
University of St Andrews
North Haugh, St Andrews, Fife KY16 9SS, UK
Prof. M. C. Gather
Centre for Nanobiophotonics
Department of Chemistry
University of Cologne
Greinstr. 4-6, 50939 Köln, Germany
Prof. A. J. C. Kuehne
DWI Leibniz Institute for Interactive Materials
Forckenbeckstraße 50, 52074 Aachen, Germany

Fluorescent nano- and microparticles represent useful entities for microscopic cellular imaging because they are readily taken up by cells via endocytosis.[1–5] If the particles carry biological recognition motifs on their surface, they can bind to specific sites in the cell, enabling molecular fluorescence labeling.[6–8] When particles exhibit a sufficiently large size, they can be used as whispering gallery mode (WGM) resonators, in which the fluorescence is amplified to the point of laser emission.[9–12] The resonator and, therefore, the size of the particle dictate the laser mode pattern and its spectral position. This feature can be used as a spectral barcode, in which slightly differently sized particles can be discerned by their individual laser spectra. In cell culture, these particles can be used to track, identify, and distinguish living cells that carry such WGM particles.[11] However, particles that are able to support WGM lasing need to be relatively large, of the order of 5–10 µm in diameter,[12] at least when made from organic materials or silica, which are the most widely used materials in this context. Therefore, such particles take up a substantial fraction of the volume available in a cell, and so there is a concern that the particles physically interfere with some of the cellular mechanisms. While the laser efficiency can be improved when increasing the amount of gain material in the particle, the resonance effect is a function of the refractive index and the size of the WGM sphere. While there are synthetic pathways that yield particles that are completely composed of conjugated polymer as a gain medium,[13,14] the refractive index of even these materials is only around $n = 1.8$, thus still requiring at least a diameter of $d = 5$ µm to support WGM lasing. However, the typical synthetic pathways to conjugated polymer particles yield only diameters in the sub-micrometer range. For a $d = 1$ µm WGM laser particle, the refractive index would need to be at least $n = 2.5$.[11] Such high refractive indices are unattainable in organic materials and are only achievable in materials that are less amenable to colloidal synthesis, such as III–V semiconductors.[15,16] A few approaches have been developed where spectrally narrow, stimulated emission has been achieved in the absence of a geometrical cavity. For instance, light with laser-like characteristics could be obtained from small micro- and nanoparticles by resonantly coupling the emission to surface plasmons or to Raman

scattering.[17–19] Stimulated resonance Raman scattering (SRRS) has been observed preferably in organic dye materials that are based on the phenylene–vinylene motif.[20–23] Interestingly, SRRS shifts with the excitation wavelength; therefore, the signal strength is less susceptible to the excitation wavelength as compared to laser emission, where the threshold and laser intensity will deteriorate with suboptimal excitation wavelengths. We have previously reported a particle-based organic laser based on poly(fluorene-co-divinylbenzene) (F8DVB).[24] F8DVB has high gain and a low threshold for amplified emission.[25] F8DVB features the above-mentioned phenylene–vinylene motif, which, together with the beneficial optical properties, could mean that the material is suitable for SRRS emission, potentially allowing us to reduce the diameter of WGM-based cell tracker particles to sizes that are smaller than 5 μm and therefore less interfering and stressful to the cell.

Here, we develop a synthetic protocol that enables the production of narrowly dispersed conjugated polymer particles, expanding the size range from sub-micrometer diameters up to several tens of micrometers. We establish that microparticles composed of F8DVB exhibit SRRS with an extremely narrow emission and an associated threshold, while we also determine the minimum particles size, which supports SRRS and WGM lasing. We show how SRRS emission can be used to image and label cells, while in combination with WGM cells can also be barcoded.

Dispersion polymerization of a step-growth type crosscoupling mechanism delivers monodisperse particles consisting entirely of conjugated polymer with very good photostability (see Figure S1 in the Supporting Information). Starting concentrations of monomer between 3.1×10^{-3} and 12×10^{-3} M deliver particles with diameters between ≈250 nm and 1.5 μm, respectively.[7,13,26] Beyond starting concentrations of ≈12×10^{-3} M, the particle diameter becomes first bidispersed and then polydisperse, preventing controlled synthesis of all-conjugated polymer particles in the micrometer range. This loss in control over the dispersity is due to secondary and subsequent nucleation, debarring monodispersity. Here, we overcome this limitation by conducting the dispersion polymerization as a fed-batch process. We furnish the reactor with a stirrer bar, 1-propanol as solvent, and 90 g L^{-1} of poly(vinylpyrrolidone-co-vinyl acetate) (PVPVA) ($M_n \approx 50$ kDa) together with 100 g L^{-1} Triton X-45 as stabilizers. We add only a small amount of monomers, divinyl benzene (DVB) and dioctyl-functionalized 2,7-di-iodofluorene (F8) in equimolar ratio together with Et₃N as base and a Pd-catalyst. The amount of monomer is sufficient to achieve nucleation but not sufficient to obtain particles with diameters >1 μm. We apply technical DVB, which comes as a mixture of ortho- and para-isomers. Furthermore, DVB is contaminated with about 30% of ethyl vinylbenzene, which acts as an endcapper for the polymerization and limits the average degree of polymerization to $X_n = 11$. We have previously established that the nucleating species is a hexa- to octamer,[26] which is why we can continue to employ technical grade DVB in this study as it delivers sufficiently high X_n for particle formation. After nucleation, we continue to feed additional
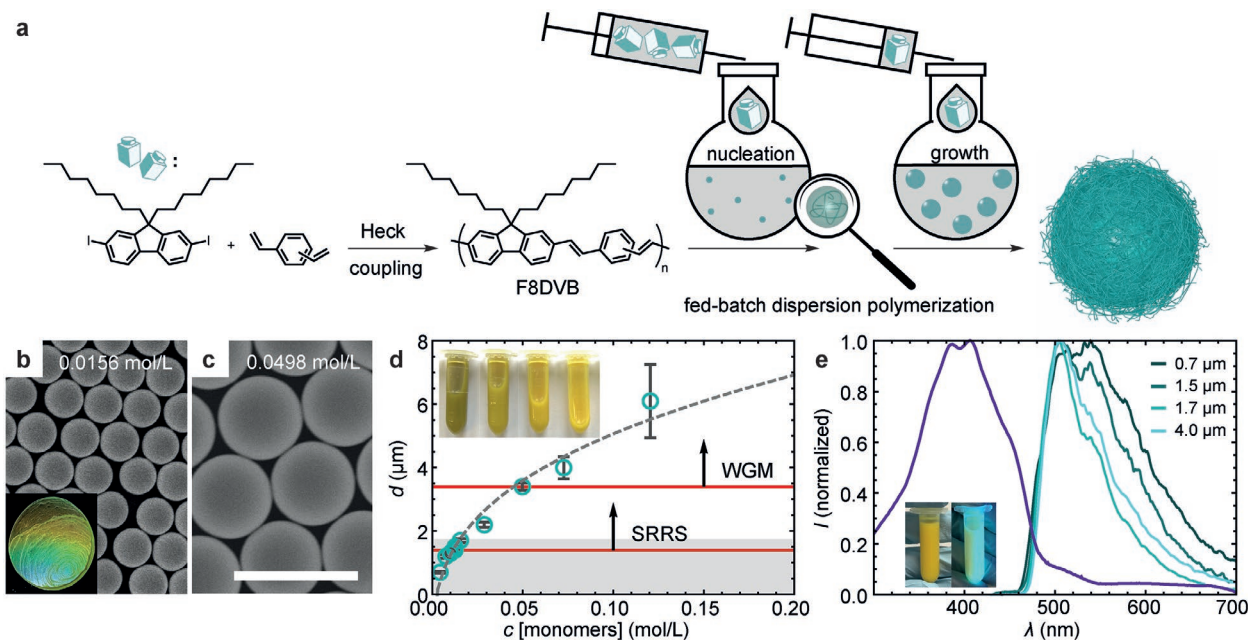

Figure 1. F8DVB particle synthesis via fed-batch dispersion polymerization. a) Reaction scheme and schematic illustration of the fed-batch dispersion polymerization for the synthesis of large F8DVB particles. b) Scanning electron microscopy (SEM) image of the particles obtained with a final concentration of 15.6×10^{-3} M. The inset shows the iridescence of self-assembled particles forming a colloidal crystal on a glass slide to provide evidence for monodispersity of the sample. c) SEM image of the particles obtained with a final concentration of 49.8×10^{-3} M. The scale bars represent 5 μm for panels (b) and (c). d) Particle diameter d as a function of the final monomer concentration. The error bars indicate the particle dispersity. Particle diameters within the gray-shaded area can be obtained from the standard batch dispersion polymerization, and sizes beyond this area can be produced in the here developed fed-batch process. The red lines are a guide to the eye. The red lines indicate the minimum particle diameter for SRRS and WGM lasing. The inset shows F8DVB particle dispersions for different particle diameters (from left to right: 0.7, 1.5, 1.7, and 4.0 μm). e) UV–vis absorption of an F8DVB film (purple line) and fluorescence of F8DVB particle dispersions in propanol (cyan lines). The inset shows an F8DVB particle dispersion in 1-propanol irradiated with white light (left) and UV light (right).
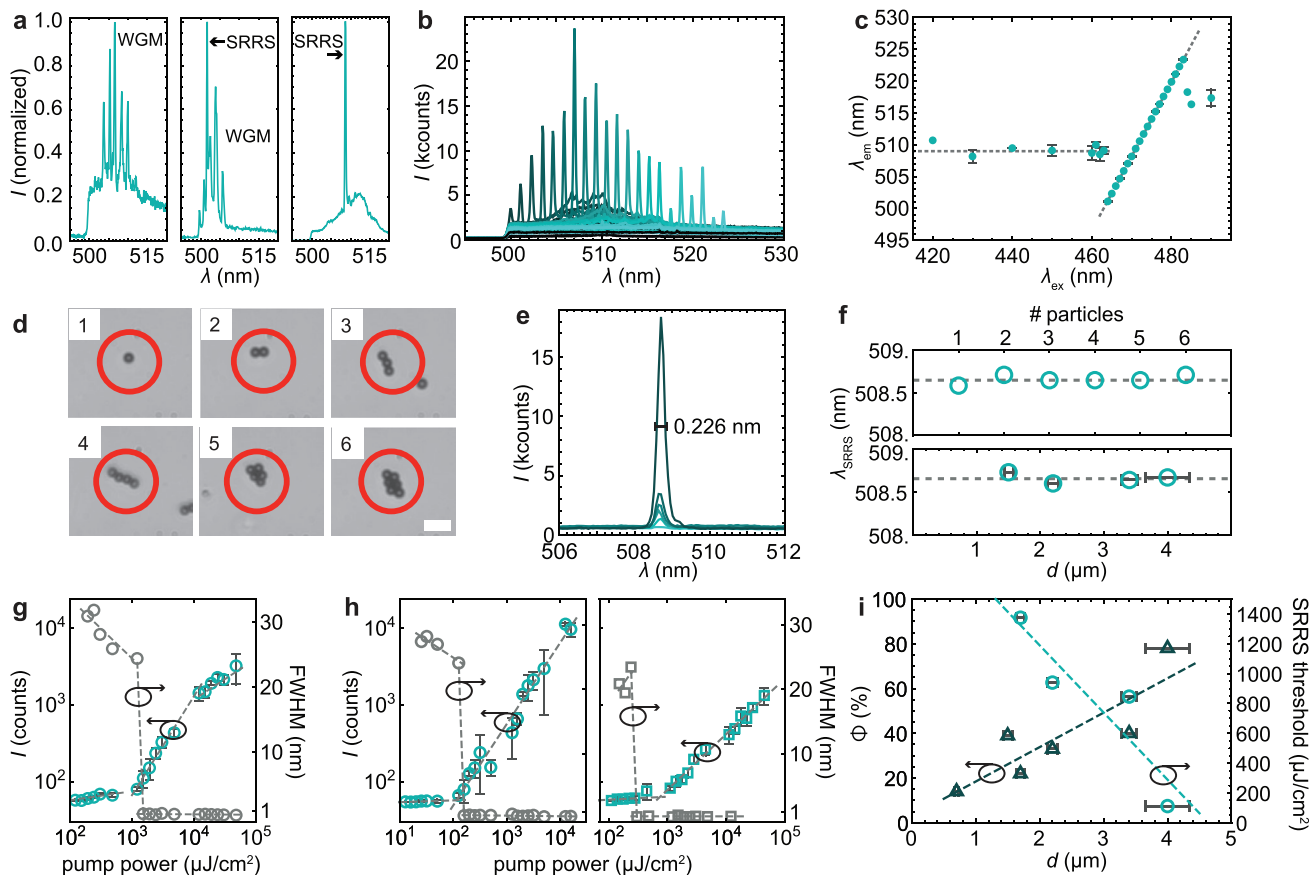
Figure 2. a) SRRS and WGM lasing in F8DVB particles. Left: Emission spectrum of a 4.0 μm particle excited at 460 nm showing WGM laser emission. Middle: Emission spectrum of a 4.0 μm particle excited at 464 nm showing WGM lasing alongside a single narrow SRRS peak at 501.7 nm. Right: Emission spectrum of a single 2.2 μm particle excited at 470 nm showing a single narrow SRRS peak at 508.5 nm. b) Overlay of the emission spectra for varying excitation wavelength λ_{ex} from 463 to 483 nm demonstrating the bathochromic shift of the SRRS peak from 500 to 520 nm for an increasing excitation wavelength. c) Emission wavelength λ_{em} of the F8DVB particles as a function of excitation wavelength λ_{ex}. The dashed line (as a guide to the eye) and the linear fit function indicate the excitation wavelength λ_{ex} ranges that can be employed to obtain WGM (below 460 nm) and SRRS (above 460 nm). d) Microscopic images of 1–6 aggregated particles ($d = 3.4$ μm). Red circles illustrate the excitation laser beam spot size. Scale bar represents 10 μm. e) Overlay of the SRRS peaks for 1–6 assembled particles (3.4 μm) excited at 470 nm, showing increasing intensity for more particles and no shift due to the absence of optical coupling. f) Top: Maxima of the respective SRRS peaks depending on the amount of assembled particles. Bottom: Maxima of SRRS peaks as a function of the particle diameter. The dashed lines mark the medians. g) SRRS threshold plot (cyan) and FWHM plot of the emission spectrum (gray) for 2.2 μm particles. h) Left: SRRS threshold plot (cyan) and FWHM plot (gray) for 4.0 μm particles. Right: WGM threshold plot and FWHM plot (gray) for 4.0 μm particles. i) Quantum yields Φ (cyan) and SRRS thresholds (gray) as a function of the particle diameters.

monomer and Et$_3$N solution at a rate of 2.0 mL h^{-1} using a syringe pump (**Figure 1**a). By keeping the monomer concentration low in the reactor, we can prevent secondary nucleation and sustain growth of the particles to much larger diameters than in a standard batch process. We can go up to final concentrations of 72.6×10^{-3} M and obtain monodisperse particles with diameters of 4 μm (Figure 1b,c; Figure S2, Supporting Information). The monodispersity is readily evidenced by the fact that the particles assemble into colloidal crystals that exhibit an optical stop band (Figure 1b, inset). Only at 120.5×10^{-3} M the particles become polydisperse with an average diameter of 6 μm (Figure 1d; Figure S2, Supporting Information). This polydispersity might be due to an increasing tendency of particle sedimentation leading to concentration inhomogeneities inside of the reactor.

Having now particles available with diameters ranging from 700 nm to >4 μm, we characterize their optical properties. We observe increasing photoluminescence quantum yields (Φ)

with increasing diameters, alongside a reduction of the $0 \rightarrow 1$ transition and more bright yellow appearance (Figures 1d (inset),e and 2i). We explain this behavior with an increasing molecular weight for larger particle diameters, as we have observed in a previous study.[26] Differential scanning calorimetry reveals that smaller particles (composed of shorter chains) exhibit higher crystallinity than larger particles (with longer chains), for which we can also resolve a glass transition temperature (see Figure S3 and Table S1 in the Supporting Information). Shorter polymers that are more likely to crystallize in the particle apparently suffer from quenching. Large particles will consist of a higher amount of polymer with greater molar mass, which tends to remain amorphous with better luminescence characteristics. When we excite individual $d = 4$ μm particles with a pulsed excitation beam (7 ns, 20 Hz) at 460 nm, we clearly observe laser emission from the conjugated polymer particles, with the characteristic WGM pattern of around 500–510 nm (Figure 2a). We check the laser

**ADVANCED
SCIENCE NEWS**
www.advancedsciencenews.com

**ADVANCED
OPTICAL
MATERIALS**
www.advopticalmat.de

emission for all of our different sizes and observe that WGM laser emission is only possible for particles with $d > 3$ µm (Figure 1d). The F8DVB particles exhibit a relatively broad absorption profile, which is why we can excite WGM laser emission using excitation wavelengths between $\lambda_{ex} = 420$ and $\lambda_{ex} = 490$ nm; however, between $\lambda_{ex} = 463$ and $\lambda_{ex} = 483$ nm, we observe an additional intense and narrow peak (Figure 2a, SRRS). In contrast to the WGM multiplet, this signal appears as a single narrow line, which shifts bathochromically with increasing excitation wavelength (Figure 2b,c). The additional sharp line shifts between $\lambda_{em} = 500$ and $\lambda_{em} = 525$ nm and scales linearly with the excitation wavelength following $\lambda_{em} = 1.17\,\lambda_{ex} - 39.41$ nm (obtained by a linear fit of the experimental data), which suggests that the additional peak is the result of SRRS (Figure 2c). The energy difference $\lambda_{em} - \lambda_{ex}$ corresponds to the stretching vibration energy of the π-conjugated phenylene–vinylene backbone, which in SRRS couples to the electronic transition within the gain spectrum of our particles.[27] To demonstrate that the observed effect is not due to mode shifting induced by coupling of multiple aggregated WGM resonators, we take spectra of a growing number of aggregated F8DVB particles and observe the sharp mode (Figure 2d,e). The assigned narrow emission line simply grows in intensity and remains at the same wavelength with an increasing number of aggregated particles, substantiating that this peak is produced by SRRS, and coupling phenomena between particles do not play a role (Figure 2f). Interestingly, we observe SRRS also for particles with $d < 3$ µm that are too small to support WGM lasing. The peak position of SRRS (λ_{SRRS}) is independent of the number of aggregated particles or the particle diameter (Figure 2f; the SRRS spectra in Figure S4, Supporting Information).

In contrast to real laser emission, SRRS does not require a population inversion; instead, the excitation needs to be strong enough to induce the required molecular vibrations to enable coupling with the emission. Therefore, a threshold can also be assigned to the input–output curve of SRRS emission (Figure 2g). The threshold of the input–output curve is accompanied by a sharp drop in the full width at half maximum (FWHM) of the emission spectrum to <1 nm, similar to the spectral behavior of laser radiation above threshold (Figure 2f). For particles that do not support WGM laser emission, the SRRS threshold is of the order of 10^3 µJ cm^{-2} (Figure 2g). We do not detect SRRS emission for particles $d < 1.4$ µm, which is most probably due to the increased crystalline content for particles below this diameter, as discussed above, preventing the required vibrational resonance and reducing the requisite gain as indicated by the deterioration of Φ with the decreasing particle diameter (Figure 2i). However, the SRRS threshold decreases with the increasing particle diameter (Figure 2h,i; Figure S5, Supporting Information). Particles with $d = 4$ µm exhibit an SRRS threshold of $O \approx 10^2$ µJ cm^{-2} that is smaller by an order of magnitude compared to $d = 2.2$ µm particles. These larger particles can support WGM laser emission, which has its own threshold of $O \approx 10^3$ µJ cm^{-2}. Depending on the excitation wavelength and the excitation power, WGM lasing, SRRS emission, or simultaneous emission can be provoked (Figure 2a). The slopes of the input–output curves are superlinear, however, relatively flat compared to other organic gain materials. This low efficiency is characteristic for F8DVB, which exhibits exciton–exciton quenching above threshold.[28–30] Again, thresholds for

lasing in the respective input–output curve come with a sharp decrease in FWHM, which decreases at the threshold to <1 nm, indicating stimulated and amplified emission.

WGM laser particles can act as barcodes, where the laser spectrum can be used to identify living cells in culture.[9–11] Our particles are capable of laser-like SRRS emission at much smaller diameters and, therefore, have the potential to give a similar response, however, at a much smaller size, meaning that the particles will not interfere with or deform the cells as strongly as particles that support WGM laser emission. To prove that our particles are fit for intracellular application, we expose our particles to macrophages differentiated from THP-1 cells, which endocytose the particles in their direct vicinity (**Figure 3**a–c). The polymerization mechanism leading to the particles might entail heavy metal Pd residues originating from catalyst that precipitates with the polymer. Inductively coupled plasma optical emission spectrometry (ICP-OES) elemental analysis provides residual amounts of only 1 wt% of Pd in the particles (see Table S2 in the Supporting Information). To confirm that this low amount of Pd is not jeopardizing cell compatibility of our particles, we perform cytotoxicity tests on our macrophages as well as on HeLa cells to prove that the particles are fully cell compatible (see Figure S6 in the Supporting Information).

Particles with diameter of $d = 2.2$ µm are taken up by macrophages almost at the same rate as particles with $d = 4$ µm (cf., Figure 3b,c). Within minutes, the macrophages take up one or more particles into the cytoplasm (see Figure S7 and Video S1 in the Supporting Information), which has no apparent effect on the emission properties of the particles (Figure 3a; the corresponding z-stack images in Figure S8 of the Supporting Information). While the uptake of multiple particles might be disadvantageous in WGM-based imaging and tracking applications, due to variation in resonator coupling over time, the sharp SRRS signal is independent of the number of particles inside of the cell (Figure 3d). We showcase this behavior by choosing five cells with one or more particles in the cytoplasm and measuring the emission after excitation above the SRRS threshold. Indeed, we observe the same narrow SRRS peak at the same spectral position for all tested cells (Figure 3d). This enables simplified staining protocols as the particle concentration does not need to be adjusted as precisely as in other staining methods, where the number of particles has to be below the cell number to prevent multiple uptake events by the same cell. Furthermore, the narrow emission signal of the particles reduces crosstalk with other emitters and frees up spectral range for other dyes and particles that can be applied for multicolor imaging and tracking of cells. While small particles of down to 1.4 µm can now be used to track cells by SRRS, larger particles can support WGM resonance and can, therefore, be used for barcoding of cells. Here we apply particles of 4 µm that can support both WGM and SRRS emission (Figure 3c,e). The slight variation in diameters in the set of $d = 4$ µm particles entails slightly shifted WGM laser multiplets. This shift can be employed to discern and identify individual cells.[11] We chose three macrophages and record their combined WGM laser and SRRS emission. As expected, the SRRS peak is situated at an identical wavelength for the three different cells and particles. By contrast, the additional peaks from the WGM laser emission appear around the SRRS peak. These laser signals are distinct for each particle and can therefore be used for barcoding
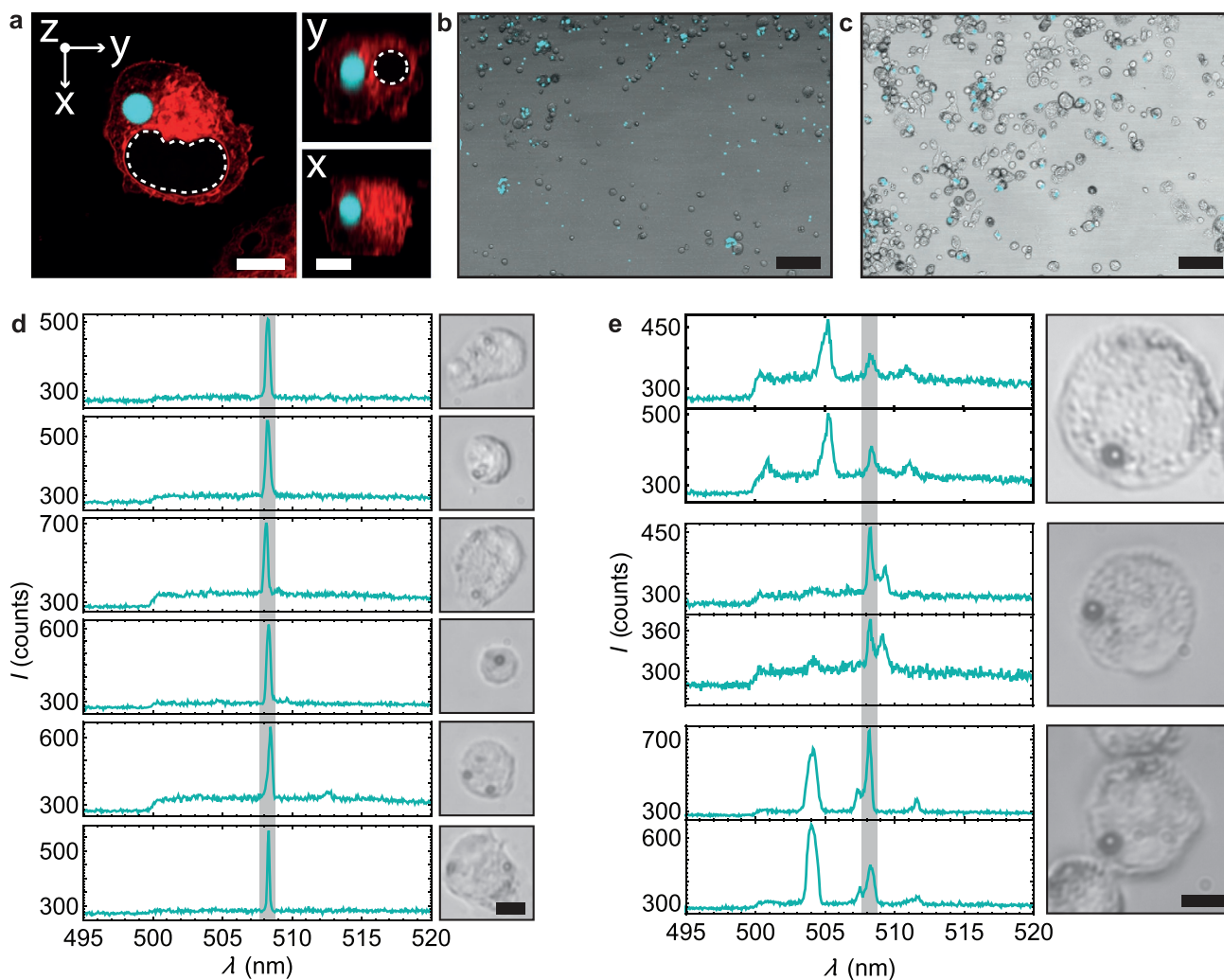
Figure 3. Live cell experiments. a) Confocal laser scanning microscopy image of a macrophage with red-stained cytoplasm, cell nucleus (highlighted by dashed line), and endocytosed F8DVB particle ($d = 3.4$ μm, cyan). The scale bar represents 6 μm. The x, y, z indices are the direction normal to the image plane. b,c) Confocal overview image (overlay of bright field and fluorescence) showing macrophages in culture that have taken up F8DVB particles are shown with cyan fluorescence with $d = 2.2$ μm (in panel (b)) and $d = 4.0$ μm. Scale bars represent 100 μm. d) Emission spectra with sharp SRRS peaks of endocytosed $d = 2.2$ μm particles and corresponding bright field images of the corresponding cells and particles. e) Emission spectra showing SRRS and WGM laser emission lines alongside of bright field images of the corresponding cells with $d = 4$ μm particles. The respective top spectrum is recorded first; the corresponding spectrum below is recorded 5 min later to indicate reproducibility of the spectral features so that the WGM spectrum can be used for cell barcoding. In panels (d) and (e), the SRRS peak is highlighted by the gray areas; $\lambda_{ex} = 470$ nm. Scale bars represent 10 μm.

of these cells. We record the emission spectra above the SRRS and WGM laser thresholds again after waiting for 5 min to let the macrophages roam on the surface and then probe them again. In this second excitation, we observe the same spectral features as in the first measurement (Figure 3e). This substantiates our claim that barcoding via WGM is also possible besides imaging and tagging using the narrow SRRS peak.

In conclusion, we have presented an optically pumped particle laser system, in which photons are simultaneously generated by population inversion and by stimulated Raman scattering in the same active medium. This enables laser-like emission from particles that are too small to support WGM resonance. In the future, this technique could be extended to other types of conjugated polymers to enable multicolor imaging, tracking, and discerning of cells. The narrow emission profile

of an SRRS emitter opens up spectral range to apply additional stains and dyes alongside the tracer particles with reduced crosstalk or undesired energy transfer.

Supporting Information

Supporting Information is available from the Wiley Online Library or from the author.

Acknowledgements

Conflict of Interest

The authors declare no conflict of interest.

Keywords

[1] X. Gao, L. Yang, J. A. Petros, F. F. Marshall, J. W. Simons, S. Nie, *Curr. Opin. Biotechnol.* **2005**, *16*, 63.

[2] M. Bradley, L. Alexander, R. M. Sanchez-Martin, *J. Fluoresc.* **2008**, *18*, 733.

[3] J. Pecher, J. Huber, M. Winterhalder, A. Zumbusch, S. Mecking, *Biomacromolecules* **2010**, *11*, 2776.

[4] A. J. C. Kuehne, *Adv. Biosyst.* **2017**, *1*, 1700100.

[5] L. P. Fernando, P. K. Kandel, J. Yu, J. McNeill, P. C. Ackroyd, K. A. Christensen, *Biomacromolecules* **2010**, *11*, 2675.

[6] K. Li, J. Pan, S. S. Feng, A. W. Wu, K. Y. Pu, Y. Liu, B. Liu, *Adv. Funct. Mater.* **2009**, *19*, 3535.

[7] N. Anwar, A. Rix, W. Lederle, A. J. C. Kuehne, *Chem. Commun.* **2015**, *51*, 9358.

[8] K. Pu, N. Chattopadhyay, J. Rao, *J. Controlled Release* **2016**, *240*, 312.

[9] M. Schubert, K. Volckaert, M. Karl, A. Morton, P. Liehm, G. B. Miles, S. J. Powis, M. C. Gather, *Sci. Rep.* **2017**, *7*, 40877.

[10] M. Humar, S. H. Yun, *Nat. Photonics* **2015**, *9*, 572.

[11] M. Schubert, A. Steude, P. Liehm, N. M. Kronenberg, M. Karl, E. C. Campbell, S. J. Powis, M. C. Gather, *Nano Lett.* **2015**, *15*, 5647.

[12] M. Kuwata-Gonokami, K. Takeda, *Opt. Mater.* **1998**, *9*, 12.

[13] A. l. J. C. Kuehne, M. C. Gather, J. Sprakel, *Nat. Commun.* **2012**, *3*, 1088.

[14] J. Pecher, S. Mecking, *Chem. Rev.* **2010**, *110*, 6260.

[15] A. H. Fikouras, M. Schubert, M. Karl, J. D. Kumar, S. J. Powis, A. Di Falco, M. C. Gather, *Nat. Commun.* **2018**, *9*, 4817.

[16] N. Martino, S. J. J. Kwok, A. C. Liapis, S. Forward, H. Jang, H. M. Kim, S. J. Wu, J. Wu, P. H. Dannenberg, S. J. Jang, Y. H. Lee, S. H. Yun, *Nat. Photonics* **2019**, *13*, 720.

[17] M. A. Noginov, G. Zhu, A. M. Belgrave, R. Bakker, V. M. Shalaev, E. E. Narimanov, S. Stout, E. Herz, T. Suteewong, U. Wiesner, *Nature* **2009**, *460*, 1110.

[18] S. Fujimoto, S. Tomita, H. Yanagi, *Jpn. J. Appl. Phys.* **2008**, *47*, 1188.

[19] E. Lafalce, Z. V. Vardeny, *Opt. Lett.* **2015**, *40*, 4699.

[20] H. Yanagi, T. Murai, S. Fujimoto, *Appl. Phys. Lett.* **2006**, *89*, 141114.

[21] S. Varghese, S. J. Yoon, E. M. Calzado, S. Casado, P. G. Boj, M. A. Díaz-García, R. Resel, R. Fischer, B. Milián-Medina, R. Wannemacher, S. Y. Park, J. Gierschner, *Adv. Mater.* **2012**, *24*, 6473.

[22] H. Yanagi, N. Kawazu, R. Takeaki, S. Tomita, K. Yamashita, K. Oe, *Synth. Met.* **2009**, *159*, 802.

[23] W. Fang, X. Shan, Z. Li, C. Sun, Z. Li, Z. Men, L. Fan, *Optik* **2012**, *123*, 1845.

[24] A. Mikosch, S. Ciftci, A. J. C. Kuehne, *ACS Nano* **2016**, *10*, 10195.

[25] T. W. Lee, O. O. Park, D. H. Choi, H. N. Cho, Y. C. Kim, *Appl. Phys. Lett.* **2002**, *81*, 424.

[26] S. Ciftci, A. J. C. Kuehne, *Macromolecules* **2015**, *48*, 8389.

[27] H. Yanagi, R. Takeaki, S. Tomita, A. Ishizumi, F. Sasaki, K. Yamashita, K. Oe, *Appl. Phys. Lett.* **2009**, *95*, 033306.

[28] Y. C. Kim, T.-W. Lee, O. O. Park, C. Y. Kim, H. N. Cho, *Adv. Mater.* **2001**, *13*, 646.

[29] R. Schroeder, W. Graupner, U. Scherf, B. Ullrich, *J. Chem. Phys.* **2002**, *116*, 3449.

[30] M. A. Baldo, R. J. Holmes, S. R. Forrest, *Phys. Rev. B: Condens. Matter Mater. Phys.* **2002**, *66*, 353211.

2001553 (6 of 6)